Research on the Mechanical Characteristics and Structural Optimization of High-Pressure Diaphragm Compressors in Hydrogen Refueling Stations under Service Conditions

Mingxin Li[1,4], Lele An[2], Wei Hu[3,*], Yudong Hou[4] and Zengli Wang[1]

[1] College of New Energy, China University of Petroleum (East China), Qingdao, 266580, China

[2] School of Rail Transit, Henan College of Transportation, Zhengzhou, 451460, China

[3] School of Mechanical Engineering, Zhengzhou University of Aeronautics, Zhengzhou, 450000, China

[4] Censtar H2-Electricity Science & Technology Zhengzhou Co., Ltd., Zhengzhou, 450046, China

INFORMATION

Keywords:
Diaphragm compressor
membrane
mechanical properties
structural optimization

DOI: 10.23967/j.rimni.2025.10.071094

SCIPEDIA Revista Internacional de Métodos Numéricos para Cálculo y Diseño en Ingeniería

Revista Internacional Métodos numéricos para cálculo y diseño en ingeniería RIMNI

In cooperation with CIMNE

Research on the Mechanical Characteristics and Structural Optimization of High-Pressure Diaphragm Compressors in Hydrogen Refueling Stations under Service Conditions

Mingxin Li[1,4], Lele An[2], Wei Hu[3,*], Yudong Hou[4] and Zengli Wang[1]

[1]College of New Energy, China University of Petroleum (East China), Qingdao, 266580, China

[2]School of Rail Transit, Henan College of Transportation, Zhengzhou, 451460, China

[3]School of Mechanical Engineering, Zhengzhou University of Aeronautics, Zhengzhou, 450000, China

[4]Censtar H2-Electricity Science & Technology Zhengzhou Co., Ltd., Zhengzhou, 450046, China

ABSTRACT

To enhance the fatigue life and service safety of the diaphragm in high-pressure diaphragm compressors, this study investigated the real-world operating conditions of hydrogen refueling station diaphragm compressors. A refined finite element model of the gas cavity cover plate–diaphragm–oil cavity support plate assembly was established using Abaqus software. Static structural analysis, thermo-structural coupling analysis, and modal analysis were conducted to examine the stress distribution of the diaphragm assembly under extreme working conditions, the influence of bolt preload on the modal characteristics of the compressor, and the effect of diaphragm thickness on stress distribution and fatigue life. The research results indicate that air holes/passages and oil holes/passages significantly affect the stress distribution of the diaphragm. The high-stress areas of the diaphragm are mainly concentrated in the transition zone of the chamber and the overlapping area between the diaphragm and the air/oil passages. The temperature inside the diaphragm compressor's membrane chamber significantly affects the stress level of the diaphragm. When the chamber temperature reaches 245°C, the maximum equivalent stress of the diaphragm reaches 1079 MPa. As the preload increases, the modal frequencies generally rise, with higher-order modes showing greater sensitivity to preload variations. Considering the stress level, fatigue life, and deflection performance of each diaphragm, the diaphragm thickness should be designed to be 0.4 mm. The finite element simulation model and research results proposed in this paper can provide a reference for the design improvement and selection of cavity types and diaphragms of diaphragm compressors in hydrogen refueling stations, as well as for the online health monitoring of hydrogen refueling stations.

OPEN ACCESS

Received: 31/07/2025

Accepted: 09/09/2025

DOI
10.23967/j.rimni.2025.10.071094

Keywords:
Diaphragm compressor
membrane
mechanical properties
structural optimization

*Correspondence: Wei Hu (huwei@zua.edu.cn).

1 Introduction

As a core component of hydrogen refueling stations, the diaphragm compressor is a volumetric compressor with a special structure, characterized by good sealing and a large compression ratio, which cannot be replaced by any other compressor [1]. The lifespan and efficiency of high-pressure diaphragm compressors directly determine the operating costs, performance, and safety of hydrogen refueling stations [2,3]. During the service process of the diaphragm compressor, the diaphragm undergoes periodic deformation between the top dead center (closely adhering to the cavity surface of the cover plate) and the bottom dead center (closely adhering to the cavity surface of the support plate and the oil distribution plate) (Fig. 1a–c) under alternating cyclic loads. The deformation is constrained by the cylinder head membrane cavity surface and the cylinder body surface, resulting in high local stress at the air holes, air passages, oil holes, and oil passages, leading to fatigue failure of the diaphragm. A large number of engineering examples from hydrogen refueling stations show that engineering problems such as premature failure due to cracks and fractures in the diaphragm (Fig. 1d–f) occur frequently, seriously affecting the operational efficiency and equipment safety of hydrogen refueling stations [4,5]. Therefore, it is urgent to explore the mechanical properties of diaphragm compressor diaphragms under real service conditions and develop structural optimization design methods to improve the fatigue life of diaphragms, reduce the probability of diaphragm failure, and enhance the efficiency and service life of diaphragm compressors.

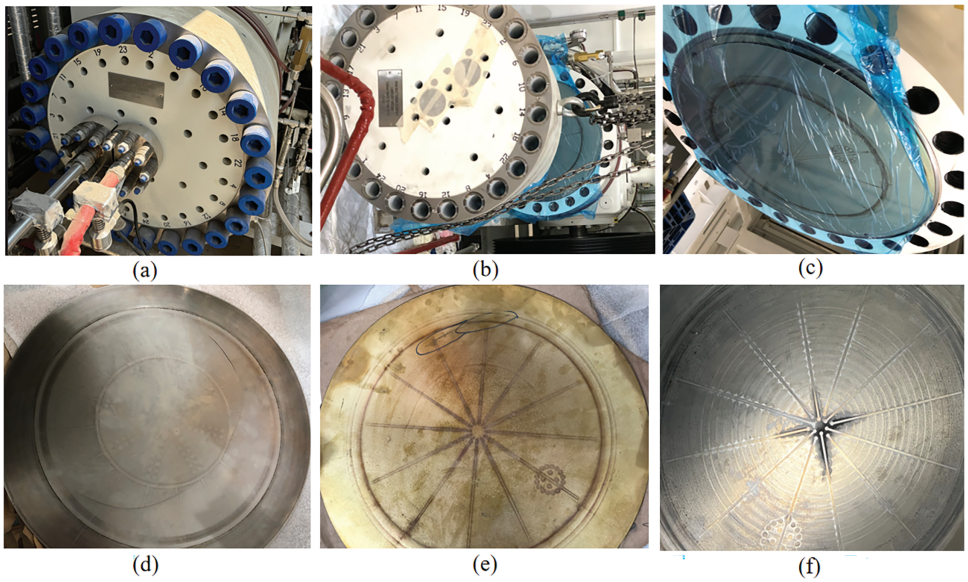

Figure 1: Typical failure modes of diaphragm compressor diaphragms: (a) diaphragm compressor, (b) diaphragm head, (c) diaphragm group, (d) diaphragm fracture, (e) copper sheet crack, (f) diaphragm crack

Currently, scholars both domestically and internationally have primarily conducted research on the mechanical properties, volumetric efficiency, diaphragm cavity structure optimization, and fault diagnosis of diaphragm compressors based on theoretical and experimental methods. Kurteev [6] conducted a detailed study on the stress and deformation of diaphragms, exploring the impact of diaphragms on the service life of air diaphragm pumps. Mathew and Hegab [7] designed the performance of a micro diaphragm compressor and analyzed the effects of materials, geometric parameters, and operating conditions on the working state of the diaphragm compressor under

constant stroke constraints. Jia et al. [8,9] found that the radial stresses under two different deflection conditions were similar, with the thickness and slot width of the diaphragm significantly affecting the radial stress. They also studied the motion pattern of the diaphragm during service. Ren et al. [10,11] investigated the mechanism by which the compressibility and temperature of hydraulic oil affect the volumetric efficiency of diaphragm compressors through a combination of theoretical analysis and experiments, and proposed corresponding optimization strategies. Zhao et al. [12–14] improved the compression efficiency of diaphragm compressors by optimizing the cavity curve. Additionally, scholars both domestically and internationally have achieved remarkable results in the field of diaphragm compressor fault diagnosis, such as the acoustic emission nondestructive diagnosis method proposed by Bayrak et al. [15,16] and the detection method for diaphragm motion state based on hydraulic oil pressure proposed by Ren et al. [17]. Scholars have also proposed methods based on characteristic event signals to identify typical abnormalities such as excessively high oil pressure, slightly insufficient oil pressure, and severely insufficient oil pressure, thereby improving the working efficiency of compressors [18,19]. Gong et al. [20,21] presented the distribution characteristics and variation laws of vacuum stress and tank strain under different internal and external pressures.

In terms of computational methods, Samaniego et al. [22] proposed a deep neural network (DNN) method based on energy functionals, which uses mechanical energy as the loss function and DNN as the approximator to solve specific partial differential equation (PDE) problems—both this method and the traditional finite element method (FEM) rely on physical laws, but the former performs calculations through numerical integration and has weak generalization ability, while the latter achieves analytical calculations via domain discretization into elements and has strong adaptability; Eshaghi et al. [23] proposed the Variational Physics-informed Neural Operator (VINO), which integrates the variational principle with neural operators and draws on the discretization idea of FEM—both VINO and traditional FEM exhibit mesh convergence, yet the former can learn global mappings to achieve fast cross-parameter prediction, while the latter requires repeated discretization calculations, resulting in lower efficiency.

Due to the frequent fatigue failure of components such as diaphragms, valves, and piston rings in diaphragm compressors, users are particularly concerned about diaphragm rupture, as it not only endangers the safety of the entire system but also requires significant maintenance time, resulting in economic losses. In response, researchers have made numerous efforts to improve the fatigue life of metal diaphragms. Wang et al. [24] found that during compressor operation, the exhaust port experiences the highest temperature, which not only leads to plastic deformation but also generates significant stress concentration. The high-temperature stress can reach the material's strength limit. To enhance the service life of the diaphragm, some scholars have investigated the influence of the contours of the gas chamber and oil chamber on the diaphragm's lifespan, and designed new chamber types to improve the diaphragm's contact state and stress distribution [13,14].

In summary, diaphragm rupture is the primary failure of diaphragm compressors and a major issue that numerous scholars are exploring solutions for. The main cause is premature fatigue fracture due to excessive additional stress generated at contact points such as air holes and oil passages between the diaphragm and the baffle plate [8]. Wear of piston rings, stall of oil pressure limiters, and drastic changes in ambient temperature can all lead to high additional stress caused by collisions between the diaphragm and the baffle plate. At the same time, due to the particularity of the hydrogen medium, strict sealing requirements are imposed on the oil chamber and gas chamber, making it difficult to accurately monitor the pressure inside the chamber and the motion pattern of the diaphragm using built-in sensors. Therefore, there is an urgent need to establish an accurate mechanical model for

diaphragm contact in diaphragm compressors to explore the motion state and stress distribution of the diaphragm.

Addressing the primary issue of diaphragm rupture and subsequent shortened lifespan in diaphragm compressors, this paper constructs a refined numerical simulation model based on the actual extreme service conditions of diaphragm compressors. It explores the mechanical properties, stress distribution, and modal variation of diaphragm compressors with pre-tightening force. On this basis, a structural optimization design method for diaphragms based on compressor compression efficiency and fatigue life is proposed [25]. This has significant engineering implications for enhancing diaphragm lifespan and reducing maintenance costs in hydrogen refueling stations. Additionally, it provides valuable references for the design improvement, selection, and long-term safe operation of core equipment in hydrogen refueling stations.

2 Models and Methods

2.1 Diaphragm Compressor Principle

The diaphragm compressor is of a top-bottom structure, primarily consisting of a cover plate, support plate, oil distribution plate, and diaphragm. The cover plate and support plate are connected by bolts, forming the upper and lower sections. The intermediate structure is a diaphragm set composed of three layers of metal diaphragms: the upper and lower layers are made of stainless steel, and the middle layer is made of copper. The diaphragm divides the diaphragm chamber into an air chamber and an oil chamber, as shown in Fig. 2. During the intake phase, the diaphragm moves to the lower dead center and comes into contact with the oil distribution plate; during the exhaust phase, the diaphragm moves to the upper dead center under the action of hydraulic oil. Stress concentration and high additional stress are generated during the contact process between the diaphragm and the air chamber and oil distribution plate, which in turn leads to fatigue damage and failure of the diaphragm.

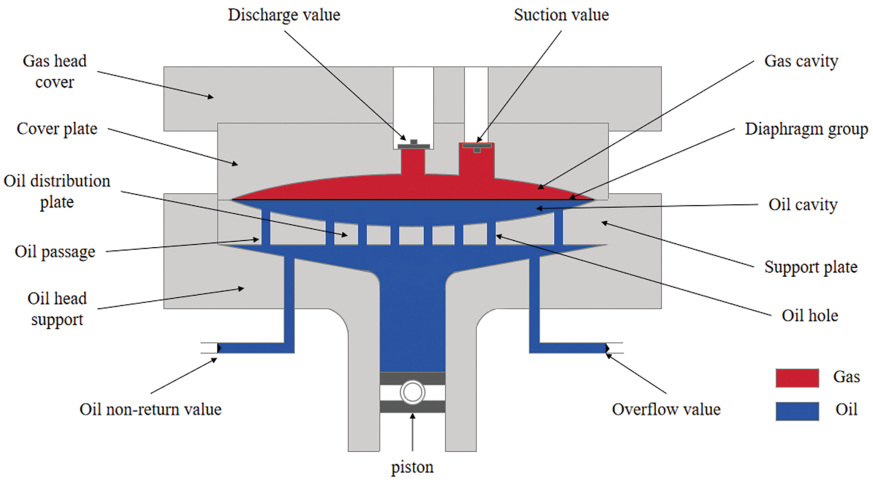

Figure 2: Diaphragm compressor membrane head structure

2.2 Experimental Methods

To accurately obtain the mechanical property parameters of the diaphragm, a static mechanical property experiment [26] was conducted on the diaphragm of a diaphragm compressor. In addition, a test system for the operating conditions of the diaphragm compressor is built to obtain its load

conditions. The installation of the test sensor is shown in Fig. 3. With a sensor sampling frequency of 200 Hz, the gas pressure sensors are installed in the intake and exhaust pipelines (close to the intake and exhaust holes), and the oil pressure sensor is installed before the relief valve, with attention paid to mounting them in straight pipe sections. Based on the monitored data, it is possible to determine whether there are faults such as abnormal pressure transmission caused by diaphragm cracks or other reasons by observing the pressure changes on the gas side and oil side (under normal operating conditions, the intake pressure shows an overall linear downward trend, while the exhaust pressure shows a linear upward trend).

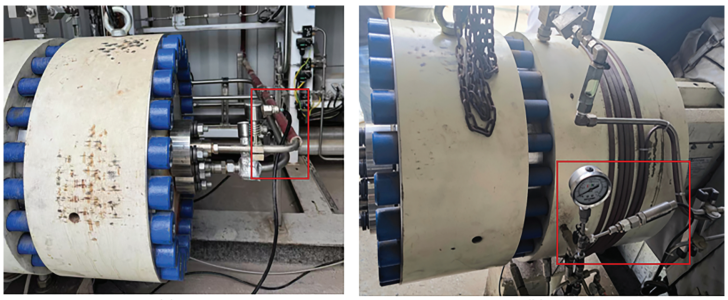

Figure 3: Load sensor installation diagram

The maximum pressure difference between the gas side and the oil side of the diaphragm measured in the experiment occurs during the exhaust stage, with the maximum pressure difference being 35 MPa. The mechanical property parameters obtained from the test experiment are presented in Table 1.

Table 1: Mechanical property parameters of oil/gas side diaphragms and intermediate diaphragms

	Gas/Oil side diaphragm	Intermediate diaphragm
Material	Inconel718 (GH4169)	Brass
Density (kg/m^3)	8190	8267
Young's modulus (MPa)	200,000	99,950
Poisson's ratio	0.300	0.345
Tensile strength (MPa)	1518	372
Yield strength (MPa)	1315	367

2.3 Numerical Simulation Model

To investigate the motion patterns and mechanical properties of the diaphragm in a diaphragm compressor under service conditions, a refined contact numerical simulation model of the diaphragm compressor's gas cavity cover plate-diaphragm group-oil cavity support plate and oil distribution plate was established based on the finite element software ABAQUS, as shown in Fig. 4. The material performance parameters of key components of the diaphragm compressor are set according to Table 1. The material model in the simulation is considered isotropic and follows an ideal elastoplastic model. The contact type between the cover plate, support plate, oil distribution plate, and diaphragm is surface-to-surface contact, and bolt preload is applied through Bolt lode.

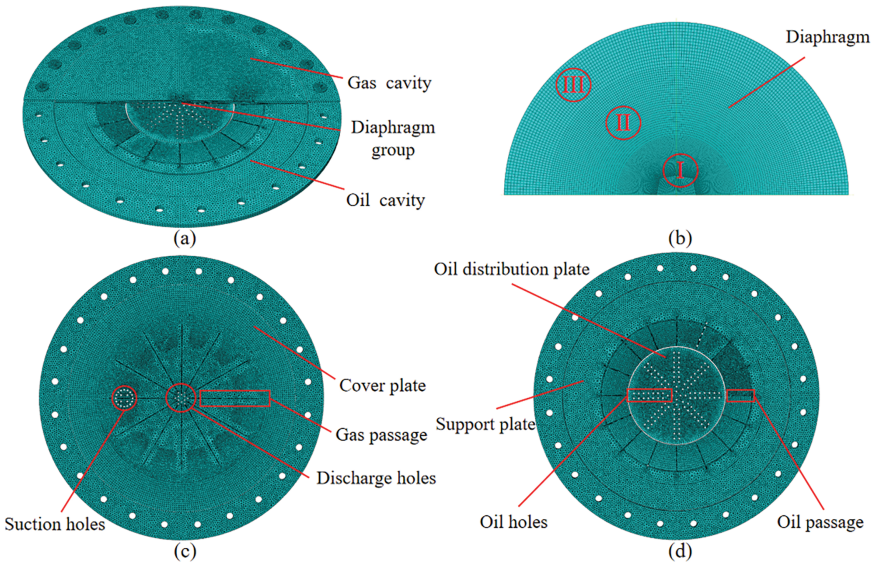

Figure 4: Numerical simulation model of diaphragm compressor gas cavity-diaphragm-oil cavity contact

In the established numerical simulation model, unstructured tetrahedral elements (specifically 10-node quadratic tetrahedrons) were adopted for meshing the cover plate, support plate, and oil distribution plate. In contrast, the diaphragm was meshed using structured hexahedral elements (8-node reduced integration hexahedrons). The initial mesh count was set to 664,648. To confirm the mesh independence of the model, a series of simulations with varying mesh counts were conducted, and the variation rate of the diaphragm's maximum stress was analyzed for comparison. The corresponding findings are presented in Table 2. As indicated in the table, when the mesh count is increased to 832,542, the stress increment rate relative to the case with 723,461 meshes is merely 0.9%. Thus, 723,461 can be regarded as the optimal mesh count. Mesh quality was further validated through comprehensive analysis checks, which covered aspects such as mesh integrity, element type compatibility, model completeness, the validity of boundary conditions, and contact pair configurations. The validation results showed that the diaphragm had a 0% error and warning rate. For other components like the cover plate, support plate, and oil distribution plate, the error rate was 0% and the warning rate was below 3%, all of which meet the computational requirements satisfactorily.

Table 2: Stress change rate under different grid numbers

Number of meshes	Stress change rate
664,648 (initial)	/
583,854	4.8%
723,461	2.1%
832,542	0.9%

2.4 Mechanical Model and Governing Equations

To clarify the physical essence and computational logic of the large deformation analysis of the circular diaphragm, this section systematically elaborates on the material constitutive relationship, large deformation governing equations, and boundary conditions. All parameters and expressions strictly correspond to the experimental and simulation scenarios of this study (material: Inconel718, subjected to static loads) to ensure model reproducibility.

2.4.1 Material Constitutive Model (Large-Deformation Linear Elasticity)

The diaphragm structure in this study is in a state of finite elastic large deformation: the material does not enter the plastic stage (subsequent simulation verification shows that the maximum stress is less than the yield strength of Inconel718, $\sigma_s = 1315$ MPa), but the displacement is comparable to the geometric dimensions (maximum deflection reaches 3–5 times its own thickness). Thus, the influence of geometric nonlinearity on mechanical responses must be considered. A Lagrangian description (with the initial configuration as the reference) is adopted to establish the constitutive relationship, and the stress-strain correlation is expressed as:

$$\boldsymbol{\sigma} = \mathbf{D} \cdot \boldsymbol{\varepsilon}^L \tag{1}$$

The definitions and specific forms of each physical quantity in the equation are as follows: $\boldsymbol{\sigma}$ is the Cauchy stress tensor, Describes the stress state in the current configuration. Due to the extremely thin thickness of the diaphragm, it is in a plane stress state (no stress in the thickness direction), with a 2D form of:

$$\boldsymbol{\sigma} = \begin{bmatrix} \sigma_{xx} & \sigma_{xy} \\ \sigma_{yx} & \sigma_{yy} \end{bmatrix} \tag{2}$$

where σ_{xx} and σ_{yy} are the normal stresses in the x- and y-directions, respectively; σ_{xy} is the shear stress. The symmetry of the stress tensor gives $\sigma_{xy} = \sigma_{yx}$.

$\boldsymbol{\varepsilon}^L$ is the Lagrangian strain tensor: considers gemeric nonlinearity under large deformation, including linear terms (contribution from small deformation) and quadratic terms (contribution from large deformation) of displacement. For the 2D plane stress state, the component expression is:

$$\boldsymbol{\varepsilon}^L = \begin{bmatrix} \varepsilon_{xx}^L \\ \varepsilon_{yy}^L \\ \varepsilon_{xy}^L \end{bmatrix} = \begin{bmatrix} \dfrac{\partial u}{\partial X} + \dfrac{1}{2}\left(\left(\dfrac{\partial u}{\partial X}\right)^2 + \left(\dfrac{\partial v}{\partial X}\right)^2\right) \\ \dfrac{\partial v}{\partial Y} + \dfrac{1}{2}\left(\left(\dfrac{\partial u}{\partial Y}\right)^2 + \left(\dfrac{\partial v}{\partial Y}\right)^2\right) \\ \dfrac{\partial u}{\partial Y} + \dfrac{\partial v}{\partial X} + \dfrac{\partial u}{\partial X}\dfrac{\partial u}{\partial Y} + \dfrac{\partial v}{\partial X}\dfrac{\partial v}{\partial Y} \end{bmatrix} \tag{3}$$

here, $u(X, Y)$ and $v(X, Y)$ are the displacement components in the x- and y-directions at the initial coordinate (X, Y) of the diaphragm; the quadratic terms are the core contribution of geometric nonlinearity under large deformation. $\mathbf{D}$ is the elasticity matrix: reflects the linear correlation between stress and strain of linear elastic materials. For the plane stress state, it is determined by the material's elastic modulus E and Poisson's ratio μ. The diaphragm material in this study is Inconel718, with measured parameters E = 200 GPa and $\mu = 0.3$. The specific form of the matrix is:

$$\mathbf{D} = \frac{E}{1-\mu^2}\begin{bmatrix} 1 & \mu & 0 \\ \mu & 1 & 0 \\ 0 & 0 & \dfrac{1-\mu}{2} \end{bmatrix} \tag{4}$$

Post-simulation processing was used to extract the maximum stress of the diaphragm $\sigma_{\max} = 439$ MPa, which is less than the yield strength of Inconel718 $\sigma_s = 1315$ MPa. Additionally, the stress-strain curve exhibits a linear relationship, confirming that the "large-deformation linear elastic constitutive model" is applicable to the scenario of this study.

2.4.2 Governing Equations (Large-Deformation Static Equilibrium)

The diaphragm in this study is analyzed for static large deformation, where inertial forces and damping forces are not considered. The governing equations are derived based on the "force equilibrium principle in the Lagrangian configuration," with the core goal of ensuring static equilibrium of any infinitesimal element in the initial configuration. The 3D form is:

$$\nabla_0 \cdot \mathbf{P} + \mathbf{b} = \mathbf{0} \quad \text{in } \Omega_0 \tag{5}$$

The definitions and application scope of each physical quantity in the equation are as follows: Ω_0 is the initial configuration domain, i.e., the geometric region of the diaphragm before loading. The diaphragm in this study is circular with an initial radius R = 222.5 mm, so the geometric description of Ω_0 is $X^2 + Y^2 \leq R^2$.

P is the 1st Piola-Kirchhoff stress tensor, which links the stress states of the initial and current configurations. It has the physical meaning of "the force per unit area in the initial configuration" and is suitable for equilibrium calculations under large deformation. For the plane stress state, the relationship between **P** and the Cauchy stress $\boldsymbol{\sigma}$ is:

$$\mathbf{P} = \boldsymbol{\sigma} \cdot \mathbf{F}^{-T} \tag{6}$$

where **F** is the deformation gradient tensor ($\mathbf{F} = \nabla_0 \mathbf{u} + \mathbf{I}$, with **I** being the identity tensor), and $\mathbf{F}^{-T}$ is the transpose of the inverse of **F**.

∇_0 is the divergence operator in the initial configuration, calculated based on the initial coordinates (X, Y). For plane problems, it simplifies to:

$$\nabla_0 \cdot \mathbf{P} = \begin{bmatrix} \dfrac{\partial P_{XX}}{\partial X} + \dfrac{\partial P_{XY}}{\partial Y} \\ \dfrac{\partial P_{YX}}{\partial X} + \dfrac{\partial P_{YY}}{\partial Y} \end{bmatrix} \tag{7}$$

where P_{XX}, P_{YY}, and P_{XY} are the components of **P**.

b is the body force vector. Only gravity is considered in this study, acting in the negative y-direction, with the expression:

$$\mathbf{b} = \begin{bmatrix} 0 \\ -\rho g \end{bmatrix} \tag{8}$$

where $\rho = 8190$ kg/m^3 (density of Inconel718) and g = 9.81 m/s^2 (gravitational acceleration).

2.4.3 Boundary Conditions

(1) Displacement Boundary

The outer edge of the diaphragm (Γ_0^u: $165.5 \leq X^2 + Y^2 \leq 222.5$ mm) is fully fixed by bolts, with no displacement in any direction. The constraint expression in the initial configuration is:

$$u(X, Y) = \begin{bmatrix} u(X, Y) \\ v(X, Y) \end{bmatrix} = \begin{bmatrix} 0 \\ 0 \end{bmatrix} \quad \forall (X, Y) \in \Gamma_0^u \tag{9}$$

In the equation, $u = 0$ and $v = 0$ denote zero displacement in the x- and y-directions, respectively.

(2) Force Boundary

A uniform pressure difference $\Delta p = 35$ MPa exists between the upper and lower surfaces of the diaphragm within a circular region with a radius $r = 165.5$ mm (the pressure direction is perpendicular to the diaphragm surface and downward). The force boundary condition is described by the dot product of the 1st Piola-Kirchhoff stress tensor $\mathbf{P}$ and the initial normal vector, with the acting region being Γ_0^u: $X^2 + Y^2 \leq 165.5$ mm. The expression is:

$$\mathbf{P} \cdot \mathbf{n}_0 = \bar{\mathbf{t}} \quad \forall (X, Y) \in \Gamma_0^t \tag{10}$$

here, $\mathbf{n}_0 = \begin{bmatrix} 0 \\ 0 \\ 1 \end{bmatrix}$ is the initial normal vector of the diaphragm surface (pointing upward), and $\bar{\mathbf{t}} = \begin{bmatrix} 0 \\ 0 \\ \Delta p \end{bmatrix}$ is the given surface force vector.

3 Result

3.1 Structural Analysis

Based on the numerical simulation model for the gas cavity-diaphragm-oil cavity contact in the diaphragm compressor (with a uniform thickness of 0.4 mm), a structural mechanical analysis was conducted. The Mises stress and radial stress distributions of the gas-side/oil-side diaphragms in the diaphragm compressor under the 35 MPa extreme working condition were obtained, as shown in Fig. 5, and the stress magnitudes are presented in Table 3. The graphs of radial stress distribution along the radial direction on both sides of the diaphragms are shown in Fig. 6.

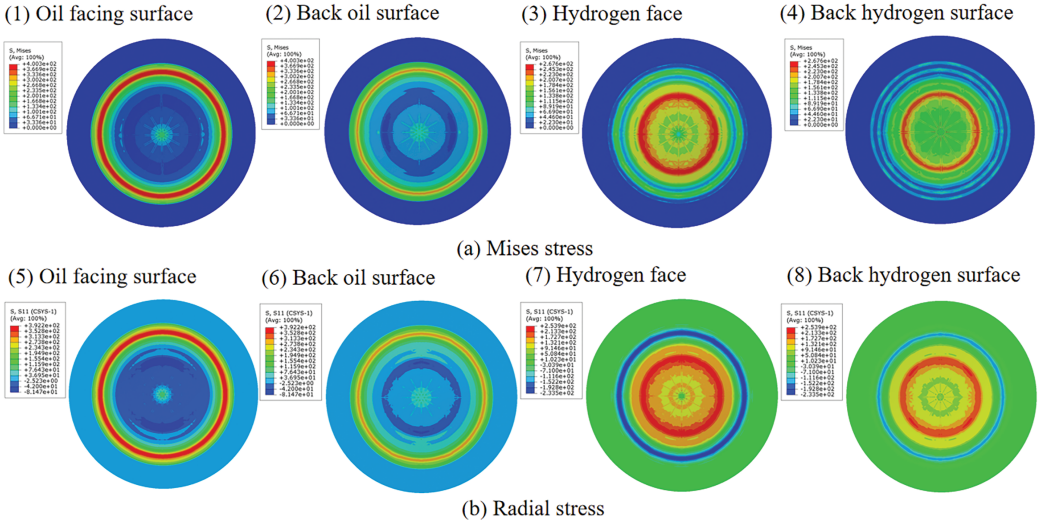

Figure 5: Contour plots of (**a**) Mises stress and (**b**) radial stress distributions on both sides of the diaphragm (gas side/oil side)

Table 3: The magnitudes of mises stress and radial stress of the gas-side and oil-side diaphragms

	Mises stress (MPa)	Radial stress (MPa)
Gas-side diaphragm	267.6	253.9
Oil-side diaphragm	400.3	392.2

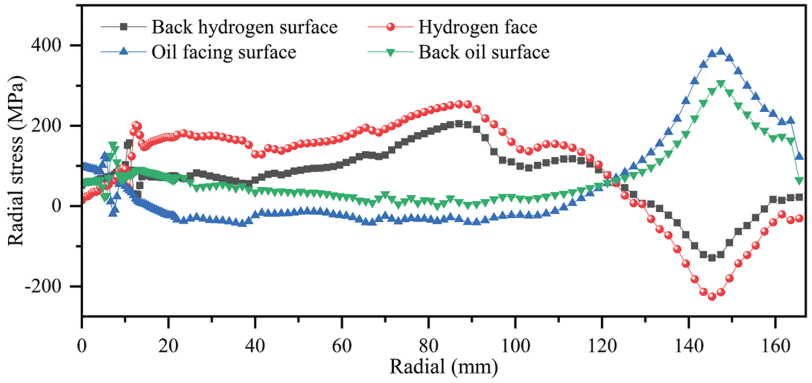

Figure 6: Graph of radial stress distribution along the radial direction on both sides of the gas-side/oil-side diaphragm

It can be seen from Figs. 5 and 6 that the maximum stress of the oil-side diaphragm occurs at its edge, with the maximum Mises stress being 400.3 MPa and the maximum radial stress being 392.4 MPa. For the hydrogen-side diaphragm, the maximum stress appears at its middle position, while the minimum stress is at the edge. The maximum Mises stress of the hydrogen-side diaphragm is 267.6 MPa, and the maximum radial stress is 253.9 MPa.

3.2 Thermal-Structure Analysis

During operation, the diaphragm compressor in a hydrogen refueling station repeatedly pressurizes hydrogen, generating a large amount of heat. Under the thermo-mechanical coupling effect, the metal diaphragm moves up and down reciprocally, with the maximum ambient temperature of the diaphragm reaching 245°C [24]. To accurately obtain the mechanical properties of the diaphragm compressor diaphragm under extreme service conditions, a numerical model for thermo-mechanical coupling analysis of the diaphragm compressor diaphragm was established. The mechanical properties of the diaphragm were investigated when the temperature of the diaphragm cavity reached 245°C.

The thermal-structure analysis adopted a direct coupling method [27], simultaneously defining mechanical and thermal boundaries using a temperature-displacement coupled analysis step. The initial ambient temperature of the model was set to 20°C. Additionally, a surface convection condition with a film coefficient of 0.1 mW/(mm^2·K) was applied to all internal cavity surfaces to define the thermal boundary conditions. Furthermore, a "To Ambient" radiation boundary condition with an emissivity of 0.6 was applied to all surfaces of the numerical model. The thermostructural parameters of the diaphragm material are listed in Table 4. The stress nephogram of the diaphragm is shown in Fig. 7.

Table 4: Diaphragm thermal parameters [28]

Parameters	100°C	200°C	300°C
Young's modulus (MPa)	196,500	193,000	181,000
Poisson's ratio	0.300	0.303	0.307
Expansion coefficient (K^{-1})	1.89E−05	1.91E−05	1.93E−05
Specific heat (mJ/(t·K))	4.52E8	4.73E8	4.89E8
Thermal Conductivity (mW/(mm·k))	14.5	16.0	17.2

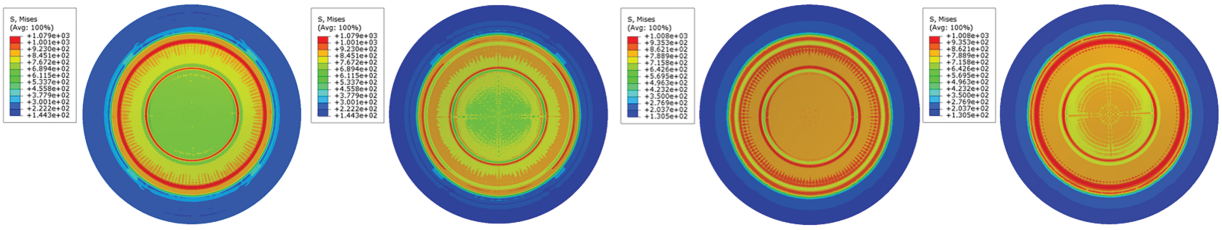

(a) Oil facing surface (b) Back oil surface (c) Hydrogen face (d) Back hydrogen surface

Figure 7: Stress distribution of the diaphragm at 245°C

3.3 Bolt Pre-Tightening Force Analysis

The cover plate and support plate of the diaphragm compressor are connected by bolts, ensuring that the diaphragm is tightened without falling off or shifting. Therefore, the tightening effect of the bolts, namely the bolt preload, will have a certain impact on the diaphragm compressor. The bolts are made of M14 nickel-chromium-aluminum alloy steel with a strength grade of 10.9. The recommended preload is 62.1 KN. When the preload is attenuated to varying degrees, the variation pattern of the first twenty modes of the diaphragm compressor is shown in Fig. 8. The abscissa 1–20 represents its first twenty modes, and the ordinate is the frequency corresponding to each mode.

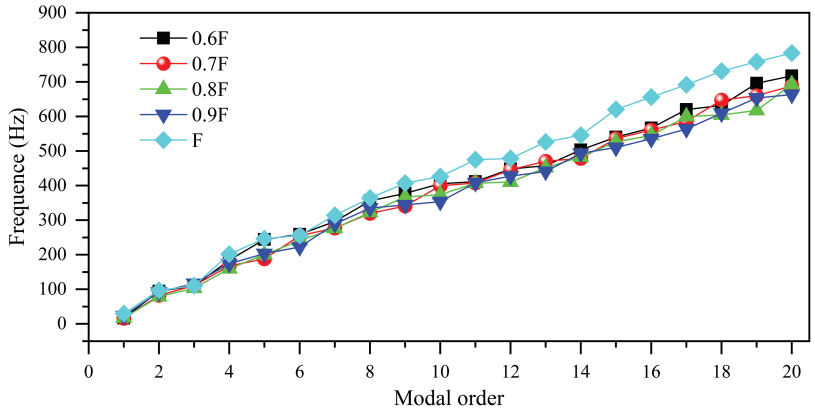

Figure 8: Influence of different pre-tightening forces on modal characteristics

3.4 Structural Parameter Optimization

The diaphragm set consists of three layers of diaphragms made of different materials, with the upper and lower layers being stainless steel and the middle layer being copper. Under the same oil-gas pressure difference, as the thickness of the diaphragm decreases, the deflection of the diaphragm also decreases, reducing the bonding points and friction points caused by interlayer impact in the central area. Therefore, reducing the thickness of the diaphragm is beneficial to lowering its stress level and improving its fatigue life. However, if the diaphragm is too thin, it may have low elasticity and be prone to fracture, while if it is too thick, its deflection and deformation performance may be poor. Therefore, considering the working conditions of the compressor comprehensively, optimizing the thickness of the diaphragm is beneficial to improving its service life.

Numerical models of air cavity-diaphragm set-oil cavity were established for different diaphragm thicknesses (the structural dimensions of the diaphragm set are shown in Table 5. Then, the diaphragm sets with different thicknesses were meshed with the same number and type of grids, and the same material properties, loads, constraints, and boundary conditions were set for finite element analysis. The stress variation pattern of the diaphragm set under extreme operating conditions is shown in Fig. 9, and the stress values for diaphragms with different thicknesses are listed in Table 5.

Table 5: Mises stress of diaphragms with different thicknesses

Diaphragm thickness (mm)	Mises stress of the oil-side diaphragm (MPa)	Mises stress of the gas-side diaphragm (MPa)
0.3	305.6	299.7
0.4	400.3	**267.6**
0.5	429	304

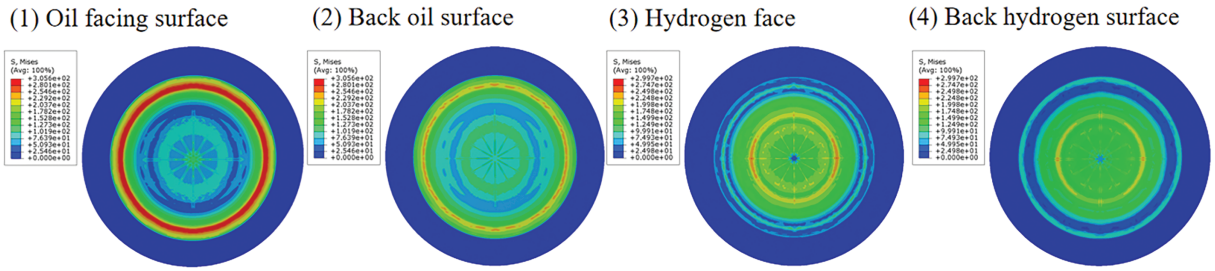

(a) 0.3mm

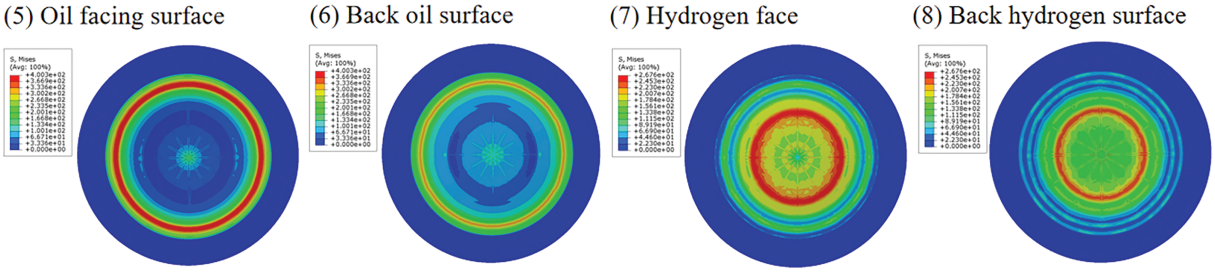

(b) 0.4mm

Figure 9: (Continued)

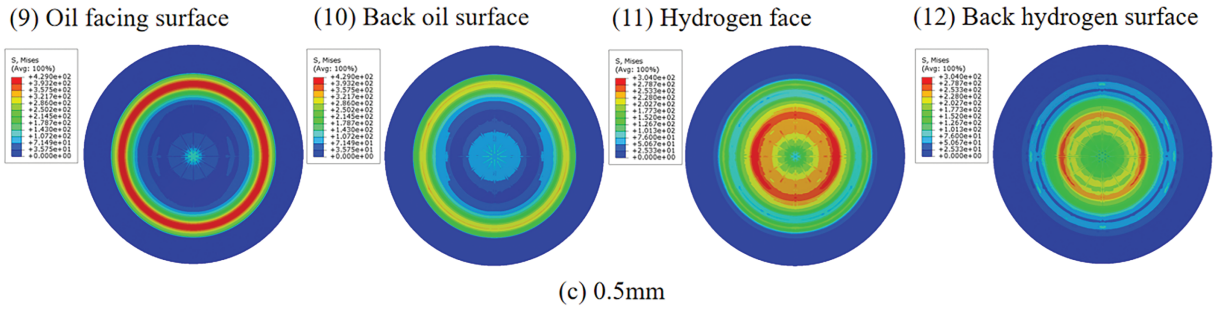

Figure 9: Stress diagram under different structural parameters of membrane groups

4 Discusses

Under extreme service conditions, the diaphragm assembly exhibits varying degrees of high stress concentration, primarily observed in the transition regions of the cavity and around the holes/slots. The oil-side diaphragm demonstrates maximum stress at its edges, with peak von Mises stress reaching 400.3 MPa and maximum radial stress of 392.4 MPa. In contrast, the hydrogen-side diaphragm shows the highest stress at its center and the lowest at the edges, recording maximum von Mises stress of 267.6 MPa and maximum radial stress of 253.9 MPa. The stress concentration occurs at the transitional edges of the cavity, which aligns with the frequently observed cracking locations during diaphragm service (Fig. 1), significantly reducing the diaphragm's service life and compromising the operational stability of the diaphragm compressor.

The results of the thermo-mechanical coupling analysis of the diaphragm compressor membrane indicate that the temperature within the membrane cavity of the diaphragm compressor has a significant impact on the stress distribution of the membrane. As the temperature of the membrane cavity increases, the stress level of the membrane significantly increases. When the cavity temperature reaches a maximum of 245°C, the stress of the gas-side membrane and the oil-side membrane increases by 277.5% and 169.7%, respectively, compared to the stress at room temperature (20°C). Among them, the oil-side diaphragm has the maximum stress, reaching 1079 MPa, which is close to the yield strength of the material (1315 MPa). Under this working condition, the stress increases significantly, which is the result of the superposition of thermal stress (caused by constrained thermal expansion) and mechanical load stress. Meanwhile, factors such as temperature gradients and changes in material properties further exacerbate this phenomenon. Therefore, in the application of diaphragm compressors, it is necessary to focus on the constraint state between the diaphragm and surrounding components, the uniformity of temperature field distribution, and the changes in the mechanical properties of materials at high temperatures to optimize the problem of a sharp increase in diaphragm stress. In addition, during the design process of the diaphragm head of the ultra-high pressure diaphragm compressor, it is essential to optimize the hydrogen cooling channels and the high-temperature early warning system to prevent excessive temperature in the diaphragm cavity from causing the diaphragm to operate under high stress, which could otherwise lead to premature fatigue damage of the diaphragm.

The results regarding the impact of different preload levels on the modal characteristics of a diaphragm compressor system indicate that the curves in the graph form a cluster that shifts upward and diverges slightly to the right as the preload increases. When considering the influence of resonance on the diaphragm compressor system, the frequency range of the first six modes is determined to be 10–260 Hz. With increasing preload, the modal frequencies generally rise, and higher-order modes

exhibit greater sensitivity to preload variations. This demonstrates that preload enhances the natural frequency of the system by strengthening the structural stiffness—an effect that is more pronounced in higher-order modes.

Optimization analysis of the diaphragm thickness in the diaphragm compressor (Fig. 9) reveals that the diaphragm thickness significantly affects the stress state of both the oil-side and gas-side diaphragms, exhibiting strong nonlinearity. The oil-side diaphragm experiences the highest stress, which increases with thickness but shows a decreasing rate of increase. Meanwhile, the gas-side diaphragm exhibits the lowest stress when its thickness is 0.4 mm. If the diaphragm is too thin, its elasticity decreases, making it prone to fracture. Conversely, if it is too thick, its flexural performance deteriorates and stress increases sharply. Considering both the fatigue life and flexural performance of the diaphragm, a thickness of 0.4 mm is reasonable.

5 Conclusions

The primary objective of this study is to determine the extreme service conditions of ultra-high-pressure diaphragm compressors in hydrogen refueling stations. Combined with mechanical property tests of the diaphragm, a high-fidelity numerical simulation model under extreme operating states was established. The research investigates the stress distribution patterns of the diaphragm under thermo-mechanical coupling conditions and examines the influence of diaphragm thickness on stress distribution. The results provide guidance and boundary conditions for the structural design and fatigue life prediction of diaphragms and membrane cavities in hydrogen refueling stations. With appropriate adjustments based on specific operational scenarios, this work may also serve as a valuable reference for research on other types of diaphragm compressors. The main conclusions are as follows:

(1) Under ambient extreme operating conditions, the maximum Mises stress and radial stress of the compressor diaphragm reach 400.3 and 392.4 MPa, respectively. High stress concentrations on both the gas and oil sides of the metal diaphragm are primarily distributed in the transition region between the cavity flange and the gas chamber, which aligns with the typical fracture locations observed during actual service. To mitigate stress concentration, the fillet radius at the starting point of the cavity profile must be optimized during the cavity generatrix design process.

(2) The thermo-mechanical coupling analysis demonstrates that elevated temperature in the diaphragm cavity significantly amplifies stress levels in both the gas-side and oil-side membranes. At 245°C, membrane stress increases by 277.5% and 169.7%, respectively, compared to room temperature conditions. This sharp rise results from the superposition of thermal stress—due to constrained thermal expansion—and mechanical load stress, exacerbated by temperature gradients and material degradation at high temperatures. To mitigate premature fatigue failure, design efforts must prioritize optimizing structural constraints, improving temperature uniformity, and accounting for high-temperature material behavior. Furthermore, enhancing hydrogen cooling channels and implementing high-temperature early-warning systems are essential to maintain safe operating conditions and extend diaphragm service life.

(3) The modal analysis of the diaphragm compressor reveals that as the preload increases, the modal frequencies generally rise, with higher-order modes exhibiting greater sensitivity to preload variations. This insight provides critical guidance for the design phase: preload should be treated as a core controllable variable, optimized to systematically enhance structural stiffness, thereby shifting the system's natural frequencies away from the primary excitation

range into a safe interval. Additionally, special attention should be paid to higher-order mode regions highly sensitive to preload to reinforce local structures.

(4) The thickness of the diaphragm significantly affects the stress state of both the oil-side and air-side diaphragms, exhibiting strong nonlinearity. The oil-side diaphragm experiences the highest stress, which increases with thickness, albeit at a decreasing rate. The air-side diaphragm has the lowest stress when its thickness is 0.4 mm. A diaphragm that is too thin has low elasticity and is prone to fracture, while a diaphragm that is too thick has deteriorated flexural performance and a sharp increase in stress. Considering both the fatigue life and flexural performance of the diaphragm, the design thickness of the diaphragm is selected as 0.4 mm.

Acknowledgement: Not applicable.

Funding Statement: The work was supported by Key Science and Technology Project in Henan Province (231111242200), National Natural Science Foundation of China (52376020), and by project ZR2024YQ014 supported by Shandong Provincial Natural Science Foundation.

Author Contributions: The authors confirm contribution to the paper as follows: Conceptualization, Mingxin Li and Wei Hu; methodology, Mingxin Li; software, Lele An; validation, Yudong Hou and Zengli Wang; formal analysis, Zengli Wang; investigation, Yudong Hou; resources, Mingxin Li; data curation, Wei Hu; writing—original draft preparation, Mingxin Li; writing—review and editing, Wei Hu; visualization, Lele An; supervision, Mingxin Li; project administration, Yudong Hou; funding acquisition, Mingxin Li. All authors reviewed the results and approved the final version of the manuscript.

Availability of Data and Materials: The datasets obtained during the current work are available from the corresponding author upon request.

Ethics Approval: Not applicable.

Conflicts of Interest: The authors declare no conflicts of interest to report regarding the present study.

References

1. Hu W. Application of domestic produced large diaphragm compressor in hydrogenation station. Energy Sci Technol. 2023;21(6):61–5. (In Chinese).
2. Li Z, Pan X, Ma J. Quantitative risk assessment on 2010 Expo hydrogen station. Int J Hydrogen Energy. 2011;36(6):4079–86. doi:10.1016/j.ijhydene.2010.12.068.
3. Balat M. Potential importance of hydrogen as a future solution to environmental and transportation problems. Int J Hydrogen Energy. 2008;33(15):4013–29. doi:10.1016/j.ijhydene.2008.05.047.
4. Li J, Zhang J, Kang Q, Jiang C. Team of bayesian optimization algorithms to solve task assignment problems in heterogeneous computing systems. In: 2014 IEEE International Conference on Systems, Man, and Cybernetics (SMC). San Diego, CA, USA: IEEE; 2014.
5. Lv R, Zhao J, Yan D, Wang J, Zhang H, Li J. Research progress on safety risk analysis and protection of core equipment in hydrogen refueling stations. Modern Chem Ind. 2025;45(2):16–20+26.
6. Kurteev VA. Diaphragms for pneumatic pumps. Chem Pet Eng. 2011;47(7–8):550–6.
7. Mathew B, Hegab H. Analytical modeling of microscale diaphragm compressors. Appl Therm Eng. 2013;51(1–2):130–6. doi:10.1016/j.applthermaleng.2012.08.052.

8. Jia X, Chen J, Wu H, Peng X. Study on the diaphragm fracture in a diaphragm compressor for a hydrogen refueling station. Int J Hydrogen Energy. 2016;41(15):6412–21. doi:10.1016/j.ijhydene.2016.02.106.
9. Jia X, Zhao Y, Chen J, Peng X. Research on the flowrate and diaphragm movement in a diaphragm compressor for a hydrogen refueling station. Int J Hydrogen Energy. 2016;41(33):14842–51. doi:10.1016/j.ijhydene.2016.05.274.
10. Ren S, Jia X, Jiang J, Zhang X, Zhao B, Peng X. Effect of hydraulic oil compressibility on the volumetric efficiency of a diaphragm compressor for hydrogen refueling stations. Int J Hydrogen Energy. 2022;47:15224. doi:10.1016/j.ijhydene.2022.03.033.
11. Ren S, Jia X, Li K, Chen F, Zhang S, Shi P, Peng X. Enhancement performance of a diaphragm compressor in hydrogen refueling stations by managing hydraulic oil temperature. Case Stud Therm Eng. 2024;53:103905. doi:10.1016/j.csite.2023.103905.
12. Zhao M, Zhang X, Yi D, Wu D. Optimization of cavity profile of diaphragm compressor based on MOPSO algorithm. Design Res. 2024;03:1–6. (In Chinese).
13. Li J, Liang L, Jia X, Peng X A new generatrix of the cavity profile of a diaphragm compressor. Proc Instit Mech Eng Part C J Mech Eng Sci. 2014;228(10):1754–66. doi:10.1177/0954406213511077.
14. Hu Y, Xu X, Wang W. A new cavity profile for a diaphragm compressor used in hydrogen fueling stations. Int J Hydrogen Energy. 2017;42(38):24458–69. doi:10.1016/j.ijhydene.2017.08.058.
15. Bayrak G. Wavelet transform-based fault detection method for hydrogen energy-based distributed generators. Int J Hydrogen Energy. 2018;43(44):20293–308. doi:10.1016/j.ijhydene.2018.06.183.
16. Li X, Chen J, Wang Z, Jia X, Peng X. A non-destructive fault diagnosis method for a diaphragm compressor in the hydrogen refueling station. Int J Hydrogen Energy. 2019;44(44):24301–11. doi:10.1016/j.ijhydene.2019.07.147.
17. Ren S, Jia X, Zhang J, Li X, Zhang S, Peng X. Diagnosis method to identify diaphragm state of diaphragm compressors for hydrogen refueling stations based on dynamic oil pressure. Int J Hydrogen Energy. 2024;49:1043–55. doi:10.1016/j.ijhydene.2023.06.214.
18. Wang Y, Brubaker K. Multi-objective model auto-calibration and reduced parameterization: exploiting gradient-based optimization tool for a hydrologic model. Environ Modell Softw. 2015;70:1–15. doi:10.1016/j.envsoft.2015.04.001.
19. Wang Y, Xue C, Jia X, Peng X. Fault diagnosis of reciprocating compressor valve with the method integrating acoustic emission signal and simulated valve motion. Mech Syst Signal Process. 2015;56:197–212. doi:10.1016/j.ymssp.2014.11.002.
20. Gong Z, Yan G, Ma J, Yan C, Shen F, Li H, et al. Vacuum loss state monitoring of aerospace vacuum pressure vessels based on quasi-distributed FBG sensing technology. Struct Durability Health Monit. 2025;19(3):473–98. doi:10.32604/sdhm.2024.057916.
21. Zhang C, Lai S, Wang H. Structural modal parameter recognition and related damage identification methods under environmental excitations: a review. Struct Durability Health Monitor. 2025;19(1):25–54. doi:10.32604/sdhm.2024.053662.
22. Samaniego E, Anitescu C, Goswami S, Nguyen T, Guo H, Hamdia K, et al. An energy approach to the solution of partial differential equations in computational mechanics via machine learning: concepts, implementation and applications. Comput Methods Appl Mech Eng. 2020;362:112790. doi:10.1016/j.cma.2019.112790.
23. Eshaghi MS, Anitescu C, Thombre M, Wang Y, Zhuang X, Rabczuk T. Variational physics-informed neural operator (VINO) for solving partial differential equations. Comput Methods Appl Mech Eng. 2025;437:117785. doi:10.1016/j.cma.2025.117785.
24. Wang T, Jia X, Li X, Ren S, Peng X. Thermal-structural coupled analysis and improvement of the diaphragm compressor cylinder head for a hydrogen refueling station. Int J Hydrogen Energy. 2020;45(1):809–21. doi:10.1016/j.ijhydene.2019.10.199.

25. Li T, Wen Z, Zhao B, Sun Q. A novel collaborative optimization assembly process method for multi-performance of aeroengine rotors. Int J Adv Manuf Technol. 2023;125:1827–43. doi:10.21203/rs.3.rs-1610736/v1.
26. Li T, Hu W, Luo H, Li M, Hou Y, Sun Q. Coupled thermal-structural analysis and structural optimization of the diaphragm of a diaphragm compressor for a hydrogen refueling station. Int J Numer Methods Calculation Design Eng. 2025;45:809–821. doi:10.1016/j.ijhydene.2019.10.199.
27. Hassan S, Stoyanov S, Rajaguru P, Bailey C. Reduced-order modelling for coupled thermal-mechanical analysis and reliability assessment of power electronic modules with nonlinear material behaviours. In: 2024 IEEE 10th Electronics System-Integration Technology Conference (ESTC); 2024 Sep 11–13; Berlin/Heidelberg, Germany. p. 1–8.
28. Dehghan S, Ismail MISB, Souri E. A thermo-mechanical finite element simulation model to analyze bushing formation and drilling tool for friction drilling of difficult-to-machine materials. J Manufact Processes. 2020;57:1004–18. doi:10.1016/j.jmapro.2020.08.046.